Published in final edited form as:
Mamm Genome. 2009 February ; 20(2): 92–108. doi:10.1007/s00335-008-9168-z.

Disruption of *Supv3L1* damages the skin, and causes sarcopenia, loss of fat, and death

Erin Paul[1], **Rachel Cronan**[1], **Paula J. Weston**[2], **Kim Boekelheide**[2], **John M. Sedivy**[1], **Sang-Yun Lee**[3], **David L. Wiest**[3], **Murray B. Resnick**[2], and **Jan E. Klysik**[1,*]

1 *Department of Molecular Biology, Cell Biology and Biochemistry, Brown University, Providence, RI 02903, USA*

2 *Department of Pathology and Laboratory Medicine, Brown University, Providence, RI,02903, USA*

3 *Fox Chase Cancer Center, Division of Basic Sciences, Philadelphia, PA 19111, USA*

Abstract

Supv3L1 is a conserved and ubiquitously expressed helicase found in numerous tissues and cell types of many species. In human cells, SUPV3L1 was shown to suppress apoptotic death, sister chromatid exchange, and impair mitochondrial RNA metabolism and protein synthesis. *In vitro* experiments revealed binding of SUPV3L1 to BLM and WRN proteins suggesting a role in genome maintenance processes. Disruption of the *Supv3L1* gene in the mouse has been reported to be embryonic lethal at early developmental stages. We generated a conditional mouse in which the phenotypes associated with the removal of exon 14 can be tested in a variety of tissues. Disruption mediated by a *Mx1* promoter-driven Cre displayed a postnatal growth delay, reduced life span, loss of adipose tissue, muscle mass, and severe skin abnormalities manifesting as ichthyosis, thickening of the epidermis, and atrophy of the dermis and subcutaneous tissue. Using a tamoxifen-activatable *Esr1*/Cre driver, *Supv3L1* disruption resulted in growth retardation and aging phenotypes including loss of adipose tissue, muscle mass, kyphosis, cachexia and premature death. Many of the abnormalities seen in the *Mx1*-Cre mice, such as hyperkeratosis characterized by profound scaling of feet and tail, could also be detected in tamoxifen-inducible Cre mice. Conditional ablation of *Supv3L1* in keratinocytes confirmed atrophic changes in the skin and ichthyosis-like changes. Together, these data indicate that Supv3L1 is important for the maintenance of the skin barrier. Additionally, loss of Supv3L1 function leads to accelerated aging-like phenotypes.

Introduction

First described in yeast (Butow et al. 1989; Conrad-Webb et al. 1990; Zhu et al. 1989), the SUV3 gene was later found to be conserved throughout evolution with orthologs documented in bacteria, plants, nematodes, *Drosophila* and mammals (Dmochowska et al. 1999). The yeast SUV3 protein localizes primarily in the mitochondrial matrix and displays RNA helicase activity (Stepien et al. 1992). Together with the ribonuclease DSS1, SUV3 forms a RNA degradosome complex (Dziembowski et al. 2003) that affects a variety of mitochondrial processes. The mammalian ortholog of the SUV3 gene, designated *Supv3L1*, is a member of the Ski2 family of DExH-box RNA helicases, and has been shown *in vitro* to possess both RNA/RNA and DNA/DNA unwinding activities (Minczuk et al. 2002; Shu et al. 2004). Although originally thought to be exclusively mitochondrial, recent evidence suggests that Supv3L1 may function both in mitochondria and in the nucleus (Minczuk et al. 2005; Shu et

*Corresponding author: Brown University, Department of Molecular Biology Cell Biology and Biochemistry, Division of Biology and Medicine, 70 Ship St., Providence, RI 02903, Tel: (401) 863-9534, FAX (401) 863-9653.

al. 2004; Szczesny et al. 2007) to modulate key cellular processes such as apoptosis (Szczesny et al. 2007), transcription, recombination and replication (Pereira et al. 2007). The predominant role of Supv3L1, however, correlates with its mitochondrial localization where it constitutes an important part of the RNA degradosome complex, whose impairment affects mitochondrial protein synthesis, reactive oxygen species (ROS) generation, ATP synthesis and mtDNA copy number (Khidr et al. 2008). The documented *in vitro* interaction of human SUPV3L1 with the BLM and WRN proteins (Pereira et al. 2007) raises the possibility that SUPV3L1 may cooperate with other genome integrity housekeepers and play an important role in genome repair and maintenance processes.

We previously reported that mouse *Supv3L1* is an important developmentally regulated gene whose disruption leads to early embryonic lethality (Pereira et al. 2007). Here, using a conditional knockout strategy, we present evidence for key functions of the gene in several adult tissues. Together, these results demonstrate that conditional disruption of *Supv3L1* leads to a premature aging phenotype, including profound skin defects resembling those found in several human skin disorders. Specifically, the *Supv3L1* helicase appears to be a contributing factor in the development of ichthyosis and psoriasis-like changes.

Materials and Methods

Targeting vector construction

Genomic DNA for vector construction was derived from MICER MHPN407c19 vector, obtained from The Welcome Trust Sanger Institute (Adams et al. 2004). The mouse genomic segment of MHPN407c19 spans 8.9kb and includes exons 13–16 of the *Supv3L1* gene [NCBI GeneID 338359]. The MICER vector was first cleaved with XhoI to remove a 5.5 kb fragment containing *Neo* resistance, and resulting plasmid (MHPN407c19ΔXhoI) was used for further modifications. The final targeting vector, pΔXhoFNFL14L, was obtained using recombineering methods (Liu et al. 2003; Warming et al. 2005) and contains a *floxed* exon 14 and a *Neo* cassette flanked with *Frt* sites (Figure1A).

Gene targeting of ES cells

129Ola ES cells derived from a male embryo were grown on mitotically inactive SNL76/7 feeder cells. 10^7 ES cells were electroporated with 20μg of pΔXhoFNFL13L linearized with AscI, and G418 selection was initiated after 24 hours. 200 G418-resistant clones were selected for further analysis. Correctly targeted ES cell clones (Figure 1B and 1C) were identified as described (Klysik and Singer 2005; Ramirez-Solis et al. 1995).

Generation of mice

All breeding and procedures were carried out at the Brown University Animal Facility according to institutional regulations and the NIH Guide for the Use and Care of Laboratory Animals. Targeted ES cells were grown to 90% confluency and harvested by trypsinization for injection. E3.5 blastocysts were derived from C57BL/C2J female mice and injected with 12–20 ES cells. The injected blastocysts were implanted into the uteri of day 2.5 pseudo-pregnant females for the generation of chimeras. 8–10 injected embryos were implanted per uterine horn. The male chimeras were mated with C57BL/C2J females to obtain F1 progeny. Germ line transmission of the *floxed* allele, designated *Supv3L1*^{tm2Jkl} (Figure 1A), was obtained with several targeted cell lines. Heterozygous *Supv3L1*^{tm2Jkl} mice were mated with B6.FVB-Tg(EIIa-cre)C5379Lmgd/J (Jackson Laboratories) to obtain the *Supv3L1*^{tm5Jkl} (Δ14) allele, or with 129S4/SVJaeSor-*Gt(ROSA)26Sor*$^{tm1(FLP1)Dym}$/J mice to remove the *Neo* cassette and obtain the *Supv3L1*^{tm3Jkl} (*floxed*) allele. Heterozygous *Supv3L1*$^{tm2Jkl/+}$ *or* *Supv3L1*$^{tm3Jkl/+}$ mice were intercrossed to generate homozygous animals carrying *floxed* exon14 (*Supv3L1*$^{tm2Jkl/tm2Jkl}$ *and Supv3L1*$^{tm3Jkl/tm3Jkl}$). Mice carrying *Supv3L1*^{tm4Jkl}

(ΔNeoΔ14) allele were obtained by crossing heterozygous *Supv3L1*$^{tm3Jkl/+}$ animals with B6.FVB-Tg(EIIa-cre)C5379Lmgd/J mice (Jackson Laboratories). In case of *Supv3L1*^{tm4Jkl} and *Supv3L1*^{tm5Jkl} (Δ14) mice, additional backcrosses to C57BL/6-*Tyr*$^{c\text{-}Brd}$ and genotyping was performed to eliminate Cre-positive animals from further use.

Mice homozygous for *Supv3L1*^{tm2Jkl} and heterozygous for an interferon-inducible Cre transgene (*Mx1*-Cre *Supv3L1*$^{tm2Jkl/tm2Jkl}$) were obtained as follows: *Supv3L1*$^{tm2Jkl/+}$ mice were crossed with the B6.Cg-Tg(Mx1-cre)1Cgn/J strain (Jackson Laboratory) and double heterozygous animals were collected. Double heterozygous mice were then mated with *Supv3L1*$^{tm2Jkl/tm2Jkl}$ and offspring was screened for *Mx1*-Cre *Supv3L1*$^{tm2Jkl/tm2Jkl}$.

The tamoxifen-inducible *Actb-Esr1*/Cre *Supv3L1*$^{tm2Jkl/tm2Jkl}$ mice were generated by crossing B6.Cg-Tg(cre/Esr1)5Amc/J mice (Jackson Laboratories) with *Supv3L1*$^{tm2Jkl/tm2Jkl}$ and screening for the *Actb-Esr1*/Cre *Supv3L1*$^{tm2Jkl/+}$ alleles. In the next step, the *Actb-Esr1*/Cre, *Supv3L1*$^{tm2Jkl/+}$ animals were crossed with *Supv3L1*$^{tm2Jkl/tm2Jkl}$ mice and *Actb-Esr1*/Cre *Supv3L1*$^{tm2Jkl/tm2Jkl}$ genotypes were selected.

The tamoxifen-inducible *Actb-Esr1*/Cre *Supv3L1*$^{tm3Jkl/tm4Jkl}$ mice were generated by crossing B6.Cg-Tg(cre/Esr1)5Amc/J mice (Jackson Laboratories) with *Supv3L1*$^{tm4Jkl/+}$ and screening for the *Actb-Esr1*/Cre *Supv3L1*$^{tm4Jkl/+}$ genotype. In the next step, *Actb-Esr1*/Cre *Supv3L1*$^{tm4Jkl/+}$ mice were crossed with *Supv3L1*$^{tm3Jkl/tm3Jkl}$ animals and the *Actb-Esr1*/Cre *Supv3L1*$^{tm3Jkl/tm4Jkl}$ genotype was selected. KRT14-Cre *Supv3L1*$^{tm3Jkl/tm4Jkl}$ mice were obtained using a similar mating strategy and the Tg(KRT14-cre/Esr1)20Efu/J strain (Jackson Laboratories). All alleles were maintained on a mixed 129/BL6 background. Since the *Supv3L1*^{tm2Jkl} and *Supv3L1*^{tm3Jkl} alleles were found to be indistinguishable in genetic crosses, survival rates and pathological assays, they will occasionally be referred to as the *Supv3L1*^{floxed} allele. Similarly, *Supv3L1*^{tm4Jkl} and *Supv3L1*^{tm5Jkl} alleles were not distinguishable and will be occasionally referred to as minus (−) allele.

Genotyping

Genomic DNA was prepared from ES cells, tail biopsies or tissues and PCR was performed using the primers shown in Figure 1D. Amplification conditions for fragments not exceeding 1kb consisted of an initial incubation at 94°C for 2 min, followed by 35 cycles at 94°C for 30 sec, 60°C for 30 sec, and 72°C for 60 sec. For longer products, the extension time at 72°C was increased by 1 min/kb.

Genotyping by Southern blotting was performed using a 598 bp PCR-generated probe (primers: AGTACTCAAGGCCAACTCTCCAACGCACC and TTCATGAAGACTGGCCTAAGGCAGACTTC) (Figure 1B).

Tamoxifen administration

4-hydroxy tamoxifen (Sigma) was prepared in ethanol at a concentration of 5 mg/ml. 40 μl of this solution was applied daily for 5 days on a shaved surface of the back skin. For subcutaneous injections tamoxifen was dissolved overnight in corn oil (Sigma) at a concentration of 20 mg/ml. The administration schedule consisted of five consecutive daily injection of 0.05 mg/gram of body weight.

Tissue processing and staining

Tissues from experimental and control littermate animals used in these studies were matched according to sex and age. Tissues were dissected out, fixed in 5% formaldehyde in PBS at 4°C, and embedded in paraffin. Hematoxylin and eosin (H&E) staining was performed by

standard procedures (Xia et al. 1999). Histological sections of tissues were analyzed by trained pathologists in a blinded fashion.

TUNEL assay

TUNEL staining for apoptotic nuclei was performed using the ApopTag Peroxidase *in situ* apoptosis detection kit (Millipore), according to the manufacturer's instructions. Labeling reactions were performed for 60 min at 37°C in a humidified chamber. Color development was accomplished using 3,3′-diaminobenzidine for 5 min. Sections were counter-stained with methyl green.

Flow cytometry

Single cell suspensions from thymus and spleen were prepared by disaggregation. Cells were washed twice with FACS wash buffer (HBSS containing 1% BSA). Before the staining, Fc-receptors were blocked for 15 min. at 4°C with anti-Fc receptor monoclonal antibody 2.4G2. Cells were then stained with monoclonal antibodies reactive with the following surface proteins: CD4, CD8, CD24, CD25, CD44, CD45, CD69, TCRβ, TCRγδ and Thy1.2. The stained cells were analyzed on a LSRII instrument (Becton Dickinson Biosciences, San Jose), using FlowJo software (Tree Star, Inc, Ashland, OR). Dead cells were excluded by propidium iodide staining.

Results

Deletion of exon 14 of the Supv3L1 gene causes lethality of homozygous embryos

We previously reported that mice heterozygous for an insertional mutation of *Supv3L1* (*Supv3L1*$^{tm1Jkl/+}$) affecting exons 11–16 are normal and fertile, while homozygous mutants displayed an early embryonic lethality (Pereira et al. 2007). The reported gene disruption also caused partial lethality of heterozygous embryos. To circumvent embryonic lethality, we developed a conditional strain carrying a *floxed* exon 14 of the *Supv3L1* gene. Exon 14 was chosen because its deletion would affect the helicase domain by causing the in-frame removal of 59 amino acids from C-terminal part of the protein. First, we confirmed that heterozygous animals carrying *Supv3L1*^{tm2Jkl}, *Supv3L1*^{tm3Jkl}, *Supv3L1*^{tm4Jkl} and *Supv3L1*^{tm5Jkl} alleles (Figure 1A) are normal up to 12 months of age and produce offspring with the expected Mendelian distribution of genotypes in backcrosses with C57BL/6 mice (not shown). This result indicates that the above mutations do not produce dominant effects including dominant negative changes. Next, intercrosses of *Supv3L1*$^{tm2Jkl/+}$ and *Supv3L1*$^{tm3Jkl/+}$ males and females were performed. These intercrosses produced pups of all three genotypes at the expected Mendelian ratios (not shown). Thus, *Supv3L1*^{tm2Jkl} as well as *Supv3L1*^{tm3Jkl} alleles could be maintained in a homozygous state, and the presence (or absence) the *Neo* cassette had no apparent effect on overall health and reproduction rates (up to 12 months of age). Since homozygous *Supv3L1*$^{tm2Jkl/tm2Jkl}$ and *Supv3L1*$^{tm3Jkl/tm3Jkl}$ animals were normal, neither floxing nor the presence of Neo cassette produced hypomorphic effects. Intercrosses of *Supv3L1*$^{tm4Jkl/+}$ or *Supv3L1*$^{tm5Jkl/+}$ animals failed to produce homozygous mice, indicating embryonic lethality caused by the removal of exon 14. Thus, disruption of both alleles by removing exon 14 confers an embryonic lethal phenotype, confirming that the *Supv3L1* gene is required during development. All together, the above genetic matings define *Supv3L1*^{tm4Jkl} and *Supv3L1*^{tm5Jkl} alleles as recessive hypomorphs, and this behavior is similar to the insertional mutation of *Supv3L1* described previously (Pereira et al. 2007). Hypomorphism appears to be the main genetic mechanism behind embryonic lethality of *Supv3L1*$^{tm4Jkl/tm4Jkl}$ and *Supv3L1*$^{tm5Jkl/tm5Jkl}$ embryos as well as conditionally induced phenotypes reported below.

Genetic crosses to produce Mx1-Cre Supv3L1$^{tm2Jkl/tm2Jkl}$ mice

The mouse *Mx1* gene is part of the viral defense system that is normally silent in healthy mice (Arnheiter et al. 1990; Horisberger and De Staritzky, 1989). In the B6.Cg-Tg(Mx1-cre)1Cgn/J transgenic strain (allele referred to hereafter as *Mx1*-Cre) the *Mx1* promoter drives the widespread expression of Cre. The *Mx1*promoter can be induced to high levels by administration of interferon alpha, interferon beta, or synthetic double-stranded RNA (Kuhn et al. 1995; Schneider et al. 2003). The genomic localization of the *Mx1*-Cre transgene was unknown at the time these studies were initiated.

As part of an effort to generate *Mx1*-Cre *Supv3L1*$^{tm2Jkl/tm2Jkl}$ animals, we crossed *Mx1*-Cre, *Supv3L1*$^{tm2Jkl/+}$ and *Supv3L1*$^{tm2Jkl/tm2Jkl}$ mice. The collected offspring (n=121) revealed almost precise partition of genotypes between *Mx1*-Cre *Supv3L1*$^{tm2Jkl/+}$ (49.58%) and *Supv3L1*$^{tm2Jkl/tm2Jkl}$ (47.1%). The low number of pups obtained for the two remaining genotypes (2.48%) was consistent with the *Mx1*-Cre transgene and *Supv3L1*^{tm2Jkl} allele being located in close proximity on homologous chromosomes, allowing the *Mx1*-Cre *Supv3L1*$^{tm2Jkl/tm2Jkl}$ and *Supv3L1*$^{tm2Jkl/+}$ genotypes to arise solely by meiotic cross-over. The position of *Supv3L1* gene is known (chromosome 10). We therefore established that the *Mx1*-Cre transgene is located on the same chromosome at a distance of approximately 2.5 cM (5Mb). To confirm close proximity of the genes, and to improve future production of experimental *Mx1*-Cre *Supv3L1*$^{tm2Jkl/tm2Jkl}$ animals, we backcrossed *Mx1*-Cre *Supv3L1*$^{tm2Jkl/+}$ males to C57BL/6-*Tyr*$^{c\text{-}Brd}$ females. Among 67 pups genotyped, one was found positive for *Mx1*-Cre and *Supv3L1*^{tm2Jkl}, confirming that a cross-over had occurred between the two loci. All together, six *Mx1*-Cre *Supv3L1*$^{tm2Jkl/tm2Jkl}$ animals were obtained from crosses of *Mx1*-Cre *Supv3L1*$^{tm2Jkl/+}$ and *Supv3L1*$^{tm2Jkl/tm2Jkl}$ mice and analyzed.

Mx1-Cre-driven Supv3L1 deletion leads to a postnatal developmental delay, skin defects, and death

The *Mx1*-Cre *Supv3L1*$^{tm2Jkl/tm2Jkl}$ animals appeared normal at birth and developed normally over the first two weeks of life. However, at weaning, signs of a developmental delay became apparent, manifested by slower growth, an abnormal appearance and density of coat hairs, and abnormally flattened and disfigured ears, as compared to the WT, *Supv3L1*$^{tm2Jkl/+}$, *Mx1*-Cre *Supv3L1*$^{tm2Jkl/+}$, or *Supv3L1*$^{tm2Jkl/tm2Jkl}$ littermates (Figure 2A). The feature of flattened and disfigured ears was used for convenient visual genotyping. At the age of four weeks the *Mx1*-Cre *Supv3L1*$^{tm2Jkl/tm2Jkl}$ animals were about half the size relative to normal littermates of other genotypes (Figure 3A). A profound scaling of the skin (ichthyosis), (Figure 2B), feet (Figure 2C), tail, and ears developed along with alopecia (Figure 2B) particularly affecting animals older than 6 weeks of age. While some animals become moribund at 4 weeks, others lived up to 10 weeks. At the time of death, all displayed adipose tissue and muscular atrophy, cachectic appearance, and failing locomotor functions. Mild kyphosis was also observed, particularly among the longer-lived individuals. The affected mice fed and drank frequently until moribund.

The shortened lifespan of *Mx1*-Cre, *Supv3L1*$^{tm2Jkl/tm2Jkl}$ mice (Figure 4A) correlated with progressive loss of exon 14. Tail biopsies taken 16, 27 and 31 days after birth revealed partial but increasing loss of exon 14 (Figure 5A). Although quantitative monitoring of gene inactivation using PCR presents obvious limitations, it nevertheless provided clear evidence that non-induced (no poly (I-C) injections were performed) and progressive deletion of exon 14 was occurring. The apparent Cre activation could be attributed either to *Mx1* promoter leakage or to endogenous production of interferon(s). The degree of exon 14 removal differed between various cell types and organs, but all tissues were found to have some *floxed* allele deleted (Figure 5B). Most notably, however, skin cells were almost totally depleted of exon 14. Testes and cerebellum appeared to display the lowest levels of *Mx1*-Cre-mediated gene damage. Pathological examination of deceased mice failed to reveal abnormalities pointing

toward a cause of death. Since animals of other genotypes (i.e. *Mx1*-Cre *Supv3L1*$^{tm2Jkl/+}$, *Supv3L1*$^{tm2Jkl/+}$, *Supv3L1*$^{tm2Jkl/tm2Jkl}$) were normal, and because of prominent signs of starvation such as adipose tissue loss, sarcopenia and cachexia, the multiple organ failure, including skin defects, could contribute to the death of *Mx1*-Cre, *Supv3L1*$^{tm2Jkl/tm2Jkl}$ mice. As the exon 14 deletion was most extensive in the skin, the pathologic changes in this organ were the most early noticeable by simple visual examination.

Mx1-Cre driven histological abnormalities in the skin

Histological examination of skin sections revealed numerous defects. The epidermis of *Mx1*-Cre *Supv3L1*$^{tm2Jkl/tm2Jkl}$ mice showed acanthosis (an increase in the thickness of the stratum spinosum), severe hyperkeratosis (a thickened stratum corneum) and hypergranulosis (an increased thickness of the granular layer) (Figure 6A, 6B and 6C). Atrophy of the dermis, muscle fibers, and adipose layers was evident along with a diminished number of hair follicles and sebaceous glands (Figure 6B). Focal parakeratosis and scaling was readily detectable in dorsal and abdominal skin (Figure 6C) and in ear cross-sections (Figure 6E and 6F). Dyskeratosis (apoptosis) in the basal layer of cells was increased and extended to the mid-epidermis. A mild dermal acute inflammatory infiltrate could be detected in longer-lived animals, but not in all cases. Dilated blood vessels were found in the dermal layer of cells of ear sections. The mixed dermal acute and chronic inflammation was more prominent in ears relative to the dorsal or abdominal skin (Figure 6E and 6F).

Histological examination of lung tissues (Figure 7A and 7B) revealed interstitial thickening caused primarily by mononuclear inflammatory cells and some polymorphonuclear neutrophils (PMNs), consistent with interstitial pneumonia, possibly contributing to death. Occasionally, foamy macrophages could be seen in the interstitium and airspaces. In the spleen, increased plasma cells in the red pulp could be detected along with increased number of foamy macrophages (Figure 7F and 7G). Histology of liver, heart and pancreas revealed no obvious histological abnormalities (not shown).

Esr1/Cre leakage results in a premature aging phenotype and death

To establish a different (tamoxifen-inducible) Cre-mediated recombination system, B6.Cg-Tg (cre/Esr1)5Amc/J transgenic mice (Jackson Laboratories) (Hayashi and McMahon 2002) were used to generate *Actb*- Esr1/Cre *Supv3L1*$^{tm2Jkl/tm2Jkl}$ and *Actb*- Esr1/Cre *Supv3L1*$^{tm3Jkl/tm4Jkl}$ animals. The *Actb*- Esr1/Cre conditional system utilizes a fusion protein composed of Cre and the ligand-binding domain of the estrogen receptor (Esr1). The estrogen receptor domain was mutated to render it unable to bind its natural ligand (17β-estradiol) but is responsive to 4-hydroxy tamoxifen (Danielian et al. 1998; Fawell et al. 1990; Littlewood et al. 1995). The estrogen receptor domain interacts with Hsp90 causing cytoplasmic sequestration of Cre/Esr1 fusion protein (Mattioni et al. 1994; Picard, 1994), thus preventing Cre-mediated recombination in the nucleus. Exposure to 4-hydroxy tamoxifen disrupts the interaction between Esr1 and Hsp90, permitting the migration of the fusion Cre/Esr1 protein to the nucleus and initiation of recombination. In the *Actb*- Esr1/Cre system, Cre/Esr1 is expressed from a chimeric promoter/enhancer of the cytomegalovirus immediate-early enhancer and the chicken-globin promoter/enhancer (*Actb*) that elicits widespread spatial expression in adult and embryonal tissues (Hayashi and McMahon 2002).

We first assessed the survival rates of *Actb*-Cre *Supv3L1*$^{tm2Jkl/tm2Jkl}$, *Actb*-Cre *Supv3L1*$^{tm3Jkl/tm4Jkl}$ and *Actb*-Cre *Supv3L1*$^{tm3Jkl/+}$ and *Actb*-Cre *Supv3L1*$^{tm2Jkl/+}$animals without administration of tamoxifen (Figure 4B). While control mice carrying one wild-type allele of *Supv3L1* were normal and no deaths were recorded in the timeframe of the experiment, the lifespan of *Actb*-Cre *Supv3L1*$^{tm2Jkl/tm2Jkl}$ and *Actb*-Cre *Supv3L1*$^{tm3Jkl/tm4Jkl}$ animals was short, averaging approximately 10 weeks. Thus, similar to *Mx1*-Cre, the *Actb*-Esr1/Cre system

displays a measurable degree of leakage causing the removal of exon 14 of the *Supv3L1* gene. The gross phenotypic appearance caused by *Actb*-Esr1/Cre leakage included kyphosis, sarcopenia and lack of fat tissue (Figure 2D). The dystrophic muscles and general cachexia led to a decline in locomotor functions (not shown). Thymic atrophy was striking (Figure 2E). The exon 14 deletion was partial and progressed to different extents in different tissues, with muscle and pancreas being the most affected (Figure 5C).

Histological examination of the skin (Figure 6G) revealed loss of adipose cells and muscle fibers. In the lung, thickening of interstitial layers of cells with focal mild chronic and acute inflammation could be detected (Figure 7C). No histopathologic changes were seen in heart muscle, liver and spleen. Thus, non-induced and *Actb*- Esr1/Cre-driven *Supv3L1* disruption leads to general dystrophic changes, many of them being reminiscent of premature aging.

Subcutaneous injection of tamoxifen enhances cachexia, kyphosis, and skin defects

Although non-induced *Actb*-Esr1/Cre leakage was sufficient to elicit clear phenotypes, it was reasonable to expect that further stimulation with tamoxifen would result in accelerated and more pronounced changes, as well as uncovering additional consequences of exon 14 removal.

The effects of subcutaneous administration of tamoxifen were tested using *Actb*-Esr1/Cre *Supv3L1*$^{tm2Jkl/tm2Jkl}$, *Actb*-Esr1/Cre *Supv3L1*$^{tm3Jkl/tm4Jkl}$ and *Actb*-Esr1/Cre *Supv3L1*$^{tm2Jkl/+}$ (control) animals at the age of 3.5 weeks. Dramatic changes in growth, adipose tissue loss, sarcopenia, thymic atrophy, kyphosis (Fig. 2F), and body weight loss were evident in *Actb*-Esr1/Cre *Supv3L1*$^{tm2Jkl/tm2Jkl}$ but not in *Actb*- Esr1/Cre *Supv3L1*$^{tm2Jkl/+}$ (control) animals. These changes occurred faster relative to non-induced changes.

The development of scales was detectable on limbs (Figure 2G) and tails. The skin of the body showed no obvious hair loss, although gene inactivation was widespread and almost complete (over 90% conversion into Δ14) in several different organs, including skin (Figure 5D). The largest fraction of intact (*floxed) Supv3L1* allele remained in the liver, spleen, lungs, duodenum and testes. Control animals (carrying one wild-type allele), displayed no tamoxifen-inducible phenotypes, yet a measurably greater loss of the *floxed* allele. This result raises the possibility that, in *Actb*- Esr1/Cre, *Supv3L1*$^{tm2Jkl/tm2Jkl}$ mice, replacement of dying cells from a pool of still unaffected stem cells (homozygous or heterozygous for exon 14) may be occurring, particularly in the spleen and liver. *Actb*- Esr1/Cre induction with tamoxifen shortened the lifespan of *Actb*- Esr1/Cre *Supv3L1*$^{tm2Jkl/tm2Jkl}$ and *Actb*- Esr1/Cre *Supv3L1*$^{tm3Jkl/tm4Jkl}$ mice (Figure 4C) and all animals died before reaching their 10th week of age.

Histopathology of skin samples isolated from tamoxifen induced *Actb*-Esr1/Cre *Supv3L1*$^{tm2Jkl/tm2Jkl}$ and *Actb*-Esr1/Cre *Supv3L1*$^{tm3Jkl/tm4Jkl}$ was different relative to untreated animals, and revealed fewer sebaceous glands, mild hyperkeratosis, acanthosis, hypergranulosis, as well as increased apoptosis in the basal layer of cells (Figure 6H). Focal vascular ectasia was evident along with an absence of adipose tissue and a greatly atrophic muscle layer. Microscopic abscesses and mild dermal acute and chronic inflammation changes were apparent. In the lung, changes such as interstitial thickening with chronic and acute inflammation and focal accumulation of foamy macrophages were found (Figure 7D and 7E). Although no obvious histological changes could be detected in the duodenum, substantially elevated levels of apoptosis were evident in the *Actb*-Esr1/Cre *Supv3L1*$^{tm3Jkl/tm4Jkl}$ (Figure 7I) relative to the control *Actb*-Esr1/Cre *Supv3L1*$^{tm3Jkl/+}$ animals (Figure 7H and 7J). Subcutaneous delivery of tamoxifen did not result in detectable alopecia.

Tamoxifen induced ablation of Supv3L1 perturbs T cell precursors in the thymus

Previous analysis indicated that conditional ablation of the Bloom syndrome (BLM) helicase, an *in vitro* interactor of Supv3L1 (Pereira et al. 2007), impaired development of T lineage cells in the thymus (Babbe et al. 2007). Accordingly, we asked whether ablation of the *Supv3L1* gene would perturb T cell development. *Actb*-Esr1/Cre *Supv3L1*$^{tm2Jkl/tm2Jkl}$, *Actb*-Esr1/Cre *Supv3L1*$^{tm3Jkl/tm4Jkl}$ and *Actb*-Esr1/Cre *Supv3L1*$^{tm2Jkl/+}$ (control) mice were injected subcutaneously with tamoxifen at the age of four weeks and thymocytes and splenocytes were isolated 10–15 days after the completion of the injection schedule. Indeed, thymic cellularity was reduced substantially (approximately 6-fold), affecting all subpopulations defined by differential expression of CD4 and CD8 (CD4−8−, CD4+8+, CD4−8+, and CD4+8−), although immature populations appeared to be preferentially depleted (Figure 8A). Among the least mature CD4−8− double negative (DN) population, the most profoundly affected subpopulations were DN3 (CD44−CD25+) and DN4 (CD44−CD25−) cells, whose survival is dependent upon signaling through the pre-T cell receptor (TCR) complex (Figure 8B) (Hoffman et al. 1996). Moreover, these effects appear to be more evident in the αβ TCR-expressing lineage than in γδ lineage DN thymocytes (Figure 8C). Immature DN3 thymocytes are induced to develop to the DN4 stage and ultimately to the CD4+8+ double positive (DP) stage by pre-TCR signaling (Fehling et al. 1995). Either this transition, or the survival of DP thymocytes is impaired by Supv3L1-deficiency, because the absolute number of DP thymocytes was reduced more than 10-fold in *Actb*-Esr1/Cre *Supv3L1*$^{tm2Jkl/tm2Jkl}$ mice (Figure 8A). TCR-induced differentiation of DP thymocytes into mature CD4+ or CD8+ single positive (SP) thymocytes appears to be less sensitive to *Supv3L1* ablation, as the absolute number of mature CD69lo thymocytes was actually increased. Likewise, mature T cells in the spleen (Figure 8F) and skin were not substantially affected. Taken together, these data suggest that immature thymocytes are sensitive to the loss of *Supv3L1* gene. This is unlikely to be an indirect effect of Supv3L1-defiency-induced stress on thymocytes, as stress-induced death of thymocytes is usually directed against DP thymocytes, whereas we also observed losses of immature DN subsets.

Topical 4-hydroxy tamoxifen application induces localized skin changes

To examine more localized, 4-hydroxy tamoxifen-inducible changes in the skin, *Actb*-Esr1/Cre *Supv3L1*$^{tm2Jkl/tm2Jkl}$ and *Actb*-Esr1/Cre *Supv3L1*$^{tm3Jkl/tm4Jkl}$ mice had the drug applied to areas of shaved back skin, a site that is not easily accessible for self-grooming, scratching and mechanical irritation. Mice were separated from their littermates and kept individually for the duration of the experiment. Seven days after completion of the treatment schedule, erythromatous reaction and scaling had developed at the application site in *Actb*-Cre *Supv3L1*$^{tm2Jkl/tm2Jkl}$ and *Actb*-Esr1/Cre *Supv3L1*$^{tm3Jkl/tm4Jkl}$ animals but not in *Actb*-Esr1/Cre *Supv3L1*$^{tm2Jkl/+}$ and *Actb*-Esr1/Cre *Supv3L1*$^{tm3Jkl/+}$ (control) mice. In the skin biopsies taken for analysis, exon 14 of the *Supv3L1* gene was efficiently deleted (Figure 5E). The subcutaneous vasculature was more prominent in the *Actb*-Esr1/Cre *Supv3L1*$^{tm2Jkl/tm2Jkl}$ skin relative to control skin. H&E staining revealed that, in the skin of animals carrying both *floxed* alleles the epidermis was thickened, revealing heperkeratosis, parakeratosis, acanthosis and hypergranulosis, while dermal blood vessels were dilated relative to *Actb*-Esr1/Cre *Supv3L1*$^{tm2Jkl/+}$ animals (Figure 6I and 6J). However, hair follicle and sebaceous gland loss was not detectable at this stage, likely because of the short period of time between 4-hydroxy tamoxifen stimulation and skin biopsy collection. This response was indistinguishable between *Actb*-Cre *Supv3L1*$^{tm2Jkl/tm2Jkl}$ and *Actb*-Esr1/Cre *Supv3L1*$^{tm3Jkl/tm4Jkl}$ animals, and therefore unrelated to the presence or absence of the *Neo* cassette (not shown).

Over time, further phenotypic changes occurred. The *Actb*-Esr1/Cre *Supv3L1*$^{tm3Jkl/tm4Jkl}$ and *Actb*-Cre *Supv3L1*$^{tm2Jkl/tm2Jkl}$ mice continued to loose weight (Figure 3B), eventually becoming sarcopenic, kyphotic and occasionally ataxic (not shown). The deletion of exon 14

appeared to be close to complete just before death in most tissues (Figure 5F), suggesting an efficient absorption of the drug through the skin. No phenotypes were detected in control mice (*Actb*-Esr1/Cre *Supv3L1*$^{tm3Jkl/+}$ or *Actb*-Cre *Supv3L1*$^{tm2Jkl/+}$) treated with 4-hydroxy tamoxifen.

Skin defects inducible by keratinocyte-specific Supv3L1 disruption

Although important in several tissues such as epithelia of the tongue, mouth, esophagus, forestomach, and the thymic epithelium, the keratin 14 (KRT14) gene is primarily expressed in keratinocytes (Lloyd et al. 1995; Moll et al. 1982; Wang et al. 1997). Thus, the KRT14 promoter is widely used to drive expression of various genes in the epidermis (Magin, 1998). To generate KRT14-Cre/Esr1 *Supv3L1*$^{tm3Jkl/tm4Jkl}$ animals we used the Tg(KRT14-Cre/Esr1) 20Efu/J strain of mice (Vasioukhin et al. 1999). These mice carry a KRT14-driven transgene encoding Cre/Esr1. Thus, upon tamoxifen administration, disruption of the *Supv3L1* gene in KRT14-Cre/Esr1 *Supv3L1*$^{tm3Jkl/tm4Jkl}$ mice can be achieved primarily in the epidermal layer of cells.

KRT14-Cre/Esr1 *Supv3L1*$^{tm3Jkl/tm4Jkl}$ and control KRT14-Cre/Esr1 *Supv3L1*$^{tm3Jkl/+}$ mice at 5 weeks of age were injected subcutaneously with tamoxifen. Three weeks later, the KRT14-Cre/Esr1 *Supv3L1*$^{tm3Jkl/tm4Jkl}$ animals showed disfiguring, erythromatous swelling of the ears while control animals appeared normal. H&E stained crossections of ear biopsies taken from a control mouse showed no apparent changes due to tamoxifen administration (Figure 6K). In contrast, ear biopsies from injected KRT14-Cre/Esr1 *Supv3L1*$^{tm3Jkl/tm4Jkl}$ animals revealed disfiguring lesions along with hyperkeratosis acanthosis, parakeratosis and scaling (Figure 6L). The epidermis was thickened, while dermal layers showed signs of chronic inflammation marked by apoptosis and the presence of focal intraepithelial lymphocyte infiltrates. Dilated blood vessels were readily detectable. KRT14-Cre/Esr1 *Supv3L1*$^{tm3Jkl/tm4Jkl}$ mice, however, did not suffer from loss of fat, muscle mass, body weight, or body hairs loss, for at least 3 months after tamoxifen administration, and no other pathological changes could be detected within this timeframe. Relative to the ears, the above changes were less pronounced in body skin. Since the keratinocyte-restricted *Supv3L1* disruption leads to dramatic changes such as hyperkeratosis, scaling, and infiltrative immune responses without apparent effects on other organ systems, Supv3L1 function is critical for the maintenance and proper function of the epidermis.

Discussion

The *Supv3L1* gene is developmentally regulated and mouse embryos carrying a homozygous insertional mutation die *in utero* before midgestation (Pereira et al. 2007). Expression of the *Supv3L1* gene in adult mammalian tissues has been reported to be widespread (Dmochowska et al. 1999). To obtain insights into the function of the Supv3L1 helicase in adult life we constructed a conditional mutation by floxing exon 14 and generated mice carrying this allele. In agreement with the previous insertional mutation we found that homozygous deletion of exon 14 in the germ line leads to an embryonic lethal phenotype, while heterozygous animals are normal and indistinguishable from their wild-type littermates for the first 12 months of life. Thus, the exon 14 removal appears to constitute a recessive hypomorphic mutation. We subsequently combined the *floxed* allele with three different Cre driver systems: two of them (*Mx1*-Cre and *Actb*-Esr1/Cre) provided widespread gene inactivation patterns corresponding with the widespread expression of *Supv3L1*, while the third one (KRT14-Cre/Esr1) was limited mostly to keratinocytes and was chosen to confirm defects in the skin. Since three different Cre drivers were applied to the same floxed allele, direct comparison of phenotypic similarities and differences between these systems was possible.

Supv3L1 gene inactivation using the Mx1-Cre system

The most striking phenotype was severe growth retardation and numerous abnormalities in the skin. A very characteristic flattening and deformity of the ears could be used with great precision for visual genotyping as early as 2–3 weeks of age. Severe alopecia and mild kyphosis were observed in animals that survived to two months. Exon 14 deletion was progressive and almost complete in the skin, while other tissues displayed a variable degree of inactivation, likely reflecting mosaic population of *Mx1*-Cre *Supv3L1*$^{tm2Jkl/tm2Jkl}$ (floxed), *Mx1*-Cre *Supv3L1*$^{tm2Jkl/tm5Jkl}$ (heterozygous), and *Mx1*-Cre *Supv3L1*$^{tm5Jkl/tm5Jkl}$ (Δ14 homozygous) cells present in these organs. Consistently, the earliest and strongest phenotypes were seen in the skin. Profound scaling developed over the entire epidermis, including feet, tail, and ears. Hyperkeratosis and focal parakeratosis were readily detectable in skin and ear cross-sections, which along with an abnormally thickened epidermis are suggestive of epidermal hyper-proliferation. Microabscesses were not frequent but occasionally evident.

One intriguing question is the mechanism of *Mx1*-Cre induction in our animals. The *Mx1* gene belongs to a family of a virus resistance loci that are silent in healthy animals but strongly induced during the interferon response to infection (Arnheiter et al. 1990). Hence, either interferon or poly(I-C) injection is typically used in the *Mx1*-Cre system to induce Cre expression, which was reported to be greatest in the liver, spleen and hematopoietic cells (close to 100%), and somewhat lower in the kidney, heart, and lung (Kuhn et al. 1995). However, we found that no induction was necessary to elicit the profound pathological changes, and ultimately death described above. A certain degree of intrinsic “leakage” of the *Mx1*-Cre system has been amply documented, but is unlikely to lead to the extensive deletion of a *floxed* allele that we have observed. One possibility is that initial deletion caused by intrinsic leakage leads to sufficient cellular damage to trigger an interferon response, thus creating a feed-forward amplifying loop. In this context it should be noted that the epidermis is the main barrier to environmental insults, and that epidermal hyperplasia often arises due to an innate immune response involving a variety of cytokines. Many of the symptoms seen in our *Mx1*-Cre *Supv3L1*$^{tm2Jkl/tm2Jkl}$ mice resemble those found in psoriasis, such as thickening of the epidermis, hyperkeratosis, parakeratosis, prominent scaling, microabsceeses and alopecia (Boehncke and Schon 2007; Gudjonsson et al. 2007; Schon, 1999). Many of these skin changes are believed to be driven by a leukocytic infiltrate composed of activated T lymphocytes, neutrophils and macrophages. Although the involvement of immunological mechanisms in the phenotypic changes observed in *Mx1*-Cre, *Supv3L1*$^{tm2Jkl/tm2Jkl}$ mice clearly requires further studies, we believe it is likely that immune cells augment *Supv3L1* deletion by supplying *Mx1*-Cre-inducing cytokines, first within the skin but subsequently also in a systemic fashion.

Supv3L1 inactivation using the Actb- Esr1/Cre and KRT14-Cre/Esr1systems

Similar to *Mx1*-Cre, in the *Actb*-Esr1/Cre system sufficient deletion of *floxed Supv3L1* occurred in the absence of exogenous induction with tamoxifen to elicit pronounced phenotypes and eventually death. The gross phenotypic changes included kyphosis, sarcopenia, complete loss of fat tissue, thymic atrophy, and atrophic changes in the skin. Administration of tamoxifen by subcutaneous injection significantly accelerated and exacerbated the development of phenotypes such as growth retardation, adipose tissue and muscle mass loss, which contributed to cachectic appearance at time of death. Severe kyphosis developed within several of weeks after drug administration. Scaling was prominent on feet and tails, a phenotype that was seen in the *Mx1*-Cre mice but did not appear in *Actb*-Esr1/Cre *Supv3L1*$^{tm2Jkl/tm2Jkl}$ or *Actb*-Esr1/Cre *Supv3L1*$^{tm3Jkl/tm4Jkl}$ mice without tamoxifen administration. In the body skin, mild hyperkeratosis was seen after induction of Cre, while no hyperkeratiosis was seen in the absence of tamoxifen. In contrast, when 4-hydroxy tamoxifen was applied topically to shaved backs of animals, severe skin phenotypes developed. The differences in the severity of the skin phenotypes elicited by different methods of Cre induction may be related to the corresponding

spatial and temporal efficiencies of *floxed* allele deletion. In addition, defects in innate immune functions, for example, occurring in the spleen and thymus due to *Supv3L1* deletion, and their subsequent effects on the responses manifested in the skin could also contribute to phenotypic differences.

A variety of additional phenotypic differences were seen in the topical and subcutaneous Cre-inducing drug delivery routes. For example, subcutaneously injected mice developed scaling of feet and tails, while topical application did not elicit such changes. The development of sarcopenia and kyphosis was seen with both of the drug delivery routes, but it was also achievable without Cre induction. Finally, when the same delivery route was applied, *Supv3L1* disruption in different genotypes (i.e. *Actb*-Esr1/Cre *Supv3L1*$^{tm2Jkl/tm2Jkl}$ and *Actb*-Esr1/Cre *Supv3L1*$^{tm3Jkl/tm4Jkl}$ mice) led to similar changes. Thus, the presence or absence of the *Neo* cassette in the targeted locus had no effect on the experimental outcome.

Keratinocyte-restricted *Supv3L1* ablation recapitulated, to a significant extent, the skin phenotypes elicited in the *Mx1*-Cre and *Actb*-Esr1/Cre systems such as ear lesions, hyperkeratosis, scaling, thickening of epidermis, dilation of blood vessels and neutrophilic infiltration. Since other organs did not suffer *Supv3L1* deletion, gross systemic phenotypes were not observed. The KRT14-Cre/Esr1system thus reinforces the notion that *Supv3L1* activity in the epidermis is important and necessary for the maintenance of its protective barrier function. Taken together, the results obtained with all three Cre-induced ablation systems strongly implicate *Supv3L1* in the maintenance of normal and healthy skin function. Immune changes resulting from compromised Supv3L1 helicase activity also warrant further examination as possible contributors in debilitating skin diseases such as psoriasis or certain forms of ichthyosis of unknown etiology.

Role of Supv3L1

Yeast Suv3 is involved in the processing of mitochondrial RNA precursors (Dziembowski et al. 2003; Margossian et al. 1996; Stepien et al. 1992). In *C. elegans*, RNAi ablation of *Suv3* is lethal at early embryonic stages (Maeda et al. 2001). Human SUPV3L1 helicase was reported to modulate apoptotic responses (Szczesny et al. 2007), elevate sister chromatid exchange, and interact with the BLM and WRN proteins (Pereira et al. 2007). However, the primary molecular function appears to involve mtRNA processing. In the absence of Supv3L1, aberrant mtRNA turnover has been shown to impair mitochondrial protein synthesis, ATP production, lower the mtDNA copy number and membrane potential, and increase the generation of ROS collectively leading to cellular senescence and cell death (Khidr et al. 2008).

Mitochondrial dysfunction can cause a wide range of disorders (Taylor and Turnbull 2005) such as progressive external ophthalmoplegia (PEO), Pearson's syndrome (PS), or Kearns Sayre syndrome (KSS). The mouse mutant of Twinkle, a nuclearly encoded mtDNA helicase displayed progressive external ophthalmoplegia, accumulation of multiple mtDNA deletions, and progressive respiratory dysfunction (Tyynismaa et al. 2005). Extensive deletions in mitochondrial DNA are believed to be the result of polymerase stalling during replication, leading to deletions forming at direct repeats (Wanrooij et al. 2004). In mtDNA diseases, the affected tissues are typically those with a high energy demand such as muscle and brain (Taylor and Turnbull 2005), resulting in symptoms similar to those associated with neurodegenerative diseases.

Although SUPV3L1 localizes primarily to the mitochondrial matrix, nuclear localization has also been well documented (Szczesny et al. 2007). BLM and WRN are well characterized genome stability housekeepers whose disruption leads to Bloom and Werner syndromes, respectively (Hickson, 2003). Genomic integrity maintenance pathways are increasingly being linked not only to a variety of diseases but also with natural as well as accelerated aging

processes. Interestingly, knockout mouse models of other helicases with important roles in DNA repair and genome maintenance display striking and overlapping phenotypic similarities to the Supv3L1 phenotypes. For example, trichothiodystrophy mice (de Boer et al. 1998) carrying a mutation in the xeroderma pigmentosum (*XPD*) gene involved in the nucleotide excision repair NER pathway show ichthyosis and hyperkeratosis, growth retardation, adipose tissue hypoplasia, reduced lifespan, and a prematurely aged appearance. Disruption of PASG (proliferation associated SNF-2-like gene) or *lsh* (lymphocyte-specific helicase), which encodes a SNF-2-like protein involved in genome methylation, causes growth retardation and premature aging symptoms such as hyperkeratosis, alopecia, reduced fat deposition, cachexia, and kyphosis (Sun et al. 2004).

There are also overlapping phenotypic similarities between knockouts of *Supv3L1* and other RecQ helicases, as well as human syndromes resulting from mutations in these genes. For example, Rothmund-Thomson syndrome (RTS), associated with mutations in the RecQL4 helicase, is clinically characterized by limb defects, frequent osteoporosis, hypogonadism, infertility, and juvenile cataracts, also displays skin changes such as congenital poikiloderma, telangiectases, atrophic hyperkeratosis, photosensitivity, and blistering (Vennos et al. 1992; Vennos and James 1995). Mouse models of RTS show growth retardation, atrophy of numerous tissues, alopecia, and scaling of the tail (Hoki et al. 2003; Mann et al. 2005). Many of these phenotypes were seen in our studies of *Supv3L1* ablation using one or more inducible Cre systems. Werner's syndrome, a premature aging disease caused by mutations in the WRN gene, is characterized by atherosclerosis, short stature, hypogonadism, premature thinning and graying leading to balding of the scalp, thin skin with telangiectases and ulceration, patchy hypopigmentation and hyperpigmentation, skin wrinkling, lymphoid depletion and thymic atrophy (Nehlin et al. 2000). The *in vitro* interaction of SUPV3L1 and WRN has been documented (Pereira et al. 2007) and some phenotypic similarities between clinical WRN features and *Supv3L1* ablated mice could be noted. Finally, clinical characteristics of Bloom syndrome include short stature, short lifespan, telangiectaticerythema in a butterfly distribution on the face in response to sun exposure, short stature, and immunodeficiency (German, 1995). Some of the Bloom characteristics overlap with those seen in our model mice, particularly short stature and short lifespan, while strong *in vitro* binding of human BLM to the SUPV3L1 protein points to importance in genome maintenance pathways (Pereira et al. 2007).

A specific human disease associated which germ line or somatic mutations in the *SUPV3L1*gene has not emerged to date. *SUPV3L1* maps to chromosome 10q22 (Rogers et al. 2000; Thomas et al. 2001), a region implicated in the hereditary motor and sensory neuropathy russe (HMSNR) syndrome, a hereditary autosomal recessive form of demyelinating motor and sensory neuropathy known as Charcot–Marie–Tooth disease type 4 (CMT4). Recent genetic studies narrowed the critical region of HMSNR to 111 kb (Hantke et al. 2003). Although these studies failed to identify the disease gene, *SUPV3L1* is present in this region, raising the possibility it may be involved in disorders affecting the peripheral nervous system. In the mouse, the widespread expression of Supv3L1 in embryonal tissues diminishes somewhat in adulthood but remains high in the brain and peripheral sensory tissues such as retina (not shown).

Depending on the tissue type and extent of *Supv3L1* gene deletion, the phenotypes of our conditional knockout mice range from severe disfiguring, ichthyosis-like, or psoriatic-like changes in the skin, to sarcopenic, premature ageing-like changes if multiple tissues are affected. Ageing mechanisms are partially understood at molecular, cellular, or organism levels. The complexity of ageing is reflected by the very large number of genes implicated in ageing progression (Slijepcevic, 2007), and numerous hypotheses that have been put forth to try to explain the molecular aspects of these phenomena. The somatic mutation theory assumes

progressive decline of cellular capacity to respond to DNA damage (Promislow, 1994). The telomere hypothesis invokes the loss of telomeric DNA as an important aspect of cellular senescence and depletion of stem cell pools (Collado et al. 2007). The oxidative stress theory implicates mitochondrial alterations in ageing (Giorgio et al. 2007), while the chromatin reorganization model implies alterations in nuclear architecture (Oberdoerffer and Sinclair 2007). Finally, the altered proteins accumulation (Terman and Brunk 2004), cellular senescence (Campisi and d'Adda di Fagagna 2007) and adult stem cells decline (Sharpless and DePinho 2007) theories were also put forward. All these models have one common denominator: the accumulation of molecular, cellular or tissue damage with age (Slijepcevic, 2007). Although germline mutation of *Supv3L1* is embryonic lethal, in a somatic environment, impaired functional activity of Supv3L1 emerges as a contributing factor that can affect processes within many of the above theoretical frameworks. The recently reported Spuv3L1-dependant processing of mammalian mtRNA molecules (Khidr et al. 2008) offers one possible, cascade-like mechanism, whose impairment may lead to mitochondrial dysfunction, consequent cellular senescence, and ultimately cell death, all of which correlate well with, and could contribute to, the phenotypic changes described in this work.

Acknowledgements

We thank Paul Monfills and Mandy Pereira for their assistance with preparation of tissue sections and collecting the images. This work was supported by a grant 5P20RR015578-07 and a grant P42ES013660 from the National Institute of Environmental Health Sciences. The content is solely the responsibility of the authors and does not necessarily represent the official views of the National Institute of Environmental Health Sciences or the National Institutes of Health.

References

1. Adams DJ, Biggs PJ, Cox T, Davies R, van der Weyden L, et al. Mutagenic insertion and chromosome engineering resource (MICER). Nat Genet 2004;36:867–871. [PubMed: 15235602]
2. Arnheiter H, Skuntz S, Noteborn M, Chang S, Meier E. Transgenic mice with intracellular immunity to influenza virus. Cell 1990;62:51–61. [PubMed: 2194673]
3. Babbe H, Chester N, Leder P, Reizis B. The Bloom's syndrome helicase is critical for development and function of the alphabeta T-cell lineage. Mol Cell Biol 2007;27:1947–1959. [PubMed: 17210642]
4. Boehncke WH, Schon MP. Animal models of psoriasis. Clin Dermatol 2007;25:596–605. [PubMed: 18021898]
5. Butow RA, Zhu H, Perlman P, Conrad-Webb H. The role of a conserved dodecamer sequence in yeast mitochondrial gene expression. Genome 1989;31:757–760. [PubMed: 2698840]
6. Collado M, Blasco MA, Serrano M. Cellular senescence in cancer and aging. Cell 2007;130:223–233. [PubMed: 17662938]
7. Conrad-Webb H, Perlman PS, Zhu H, Butow RA. The nuclear SUV3-1 mutation affects a variety of post-transcriptional processes in yeast mitochondria. Nucleic Acids Res 1990;18:1369–1376. [PubMed: 2158076]
8. Danielian PS, Muccino D, Rowitch DH, Michael SK, McMahon AP. Modification of gene activity in mouse embryos in utero by a tamoxifen-inducible form of Cre recombinase. Curr Biol 1998;8:1323–1326. [PubMed: 9843687]
9. de Boer J, de Wit J, van Steeg H, Berg RJ, Morreau H, et al. A mouse model for the basal transcription/DNA repair syndrome trichothiodystrophy. Mol Cell 1998;1:981–990. [PubMed: 9651581]
10. Dmochowska A, Kalita K, Krawczyk M, Golik P, Mroczek K, et al. A human putative Suv3-like RNA helicase is conserved between Rhodobacter and all eukaryotes. Acta Biochim Pol 1999;46:155–162. [PubMed: 10453991]
11. Dziembowski A, Piwowarski J, Hoser R, Minczuk M, Dmochowska A, et al. The yeast mitochondrial degradosome. Its composition, interplay between RNA helicase and RNase activities and the role in mitochondrial RNA metabolism. J Biol Chem 2003;278:1603–1611. [PubMed: 12426313]

12. Fawell SE, Lees JA, White R, Parker MG. Characterization and colocalization of steroid binding and dimerization activities in the mouse estrogen receptor. Cell 1990;60:953–962. [PubMed: 2317866]
13. Fehling HJ, Krotkova A, Saint-Ruf C, von Boehmer H. Crucial role of the pre-T-cell receptor alpha gene in development of alpha beta but not gamma delta T cells. Nature 1995;375:795–798. [PubMed: 7596413]
14. German J. Bloom's syndrome. Dermatol Clin 1995;13:7–18. [PubMed: 7712653]
15. Giorgio M, Trinei M, Migliaccio E, Pelicci PG. Hydrogen peroxide: a metabolic by-product or a common mediator of ageing signals? Nat Rev Mol Cell Biol 2007;8:722–728. [PubMed: 17700625]
16. Gudjonsson JE, Johnston A, Dyson M, Valdimarsson H, Elder JT. Mouse models of psoriasis. J Invest Dermatol 2007;127:1292–1308. [PubMed: 17429444]
17. Hantke J, Rogers T, French L, Tournev I, Guergueltcheva V, et al. Refined mapping of the HMSNR critical gene region--construction of a high-density integrated genetic and physical map. Neuromuscul Disord 2003;13:729–736. [PubMed: 14561496]
18. Hayashi S, McMahon AP. Efficient recombination in diverse tissues by a tamoxifen-inducible form of Cre: a tool for temporally regulated gene activation/inactivation in the mouse. Dev Biol 2002;244:305–318. [PubMed: 11944939]
19. Hickson ID. RecQ helicases: caretakers of the genome. Nat Rev Cancer 2003;3:169–178. [PubMed: 12612652]
20. Hoffman ES, Passoni L, Crompton T, Leu TM, Schatz DG, et al. Productive T-cell receptor beta-chain gene rearrangement: coincident regulation of cell cycle and clonality during development in vivo. Genes Dev 1996;10:948–962. [PubMed: 8608942]
21. Hoki Y, Araki R, Fujimori A, Ohhata T, Koseki H, et al. Growth retardation and skin abnormalities of the Recql4-deficient mouse. Hum Mol Genet 2003;12:2293–2299. [PubMed: 12915449]
22. Horisberger MA, De Staritzky K. Expression and stability of the Mx protein in different tissues of mice, in response to interferon inducers or to influenza virus infection. J Interferon Res 1989;9:583–590. [PubMed: 2794581]
23. Khidr L, Wu G, Davila A, Procaccio V, Wallace D, et al. Role of SUV3 helicase in maintaining mitochondrial homeostasis in human cells. J Biol Chem 2008;283:27064–27073. [PubMed: 18678873]
24. Klysik J, Singer JD. Mice with the enhanced green fluorescent protein gene knocked in to chromosome 11 exhibit normal transmission ratios. Biochem Genet 2005;43:321–333. [PubMed: 16144308]
25. Kuhn R, Schwenk F, Aguet M, Rajewsky K. Inducible gene targeting in mice. Science 1995;269:1427–1429. [PubMed: 7660125]
26. Littlewood TD, Hancock DC, Danielian PS, Parker MG, Evan GI. A modified oestrogen receptor ligand-binding domain as an improved switch for the regulation of heterologous proteins. Nucleic Acids Res 1995;23:1686–1690. [PubMed: 7784172]
27. Liu P, Jenkins NA, Copeland NG. A highly efficient recombineering-based method for generating conditional knockout mutations. Genome Res 2003;13:476–484. [PubMed: 12618378]
28. Lloyd C, Yu QC, Cheng J, Turksen K, Degenstein L, et al. The basal keratin network of stratified squamous epithelia: defining K15 function in the absence of K14. J Cell Biol 1995;129:1329–1344. [PubMed: 7539810]
29. Maeda I, Kohara Y, Yamamoto M, Sugimoto A. Large-scale analysis of gene function in Caenorhabditis elegans by high-throughput RNAi. Curr Biol 2001;11:171–176. [PubMed: 11231151]
30. Magin TM. Lessons from keratin transgenic and knockout mice. Subcell Biochem 1998;31:141–172. [PubMed: 9932492]
31. Mann MB, Hodges CA, Barnes E, Vogel H, Hassold TJ, et al. Defective sister-chromatid cohesion, aneuploidy and cancer predisposition in a mouse model of type II Rothmund-Thomson syndrome. Hum Mol Genet 2005;14:813–825. [PubMed: 15703196]
32. Margossian SP, Li H, Zassenhaus HP, Butow RA. The DExH box protein Suv3p is a component of a yeast mitochondrial 3′-to-5′ exoribonuclease that suppresses group I intron toxicity. Cell 1996;84:199–209. [PubMed: 8565066]
33. Mattioni T, Louvion JF, Picard D. Regulation of protein activities by fusion to steroid binding domains. Methods Cell Biol 1994;43(Pt A):335–352. [PubMed: 7823870]

34. Minczuk M, Mroczek S, Pawlak SD, Stepien PP. Human ATP-dependent RNA/DNA helicase hSuv3p interacts with the cofactor of survivin HBXIP. Febs J 2005;272:5008–5019. [PubMed: 16176273]
35. Minczuk M, Piwowarski J, Papworth MA, Awiszus K, Schalinski S, et al. Localisation of the human hSuv3p helicase in the mitochondrial matrix and its preferential unwinding of dsDNA. Nucleic Acids Res 2002;30:5074–5086. [PubMed: 12466530]
36. Moll R, Franke WW, Schiller DL, Geiger B, Krepler R. The catalog of human cytokeratins: patterns of expression in normal epithelia, tumors and cultured cells. Cell 1982;31:11–24. [PubMed: 6186379]
37. Nehlin JO, Skovgaard GL, Bohr VA. The Werner syndrome. A model for the study of human aging. Ann NY Acad Sci 2000;908:167–179. [PubMed: 10911957]
38. Oberdoerffer P, Sinclair DA. The role of nuclear architecture in genomic instability and ageing. Nat Rev Mol Cell Biol 2007;8:692–702. [PubMed: 17700626]
39. Pereira M, Mason P, Szczesny RJ, Maddukuri L, Dziwura S, et al. Interaction of human SUV3 RNA/DNA helicase with BLM helicase: loss of the SUV3 gene results in mouse embryonic lethality. Mech Aging Dev 2007;128:609–617. [PubMed: 17961633]
40. Picard D. Regulation of protein function through expression of chimaeric proteins. Curr Opin Biotechnol 1994;5:511–515. [PubMed: 7765465]
41. Promislow DE. DNA repair and the evolution of longevity: a critical analysis. J Theor Biol 1994;170:291–300. [PubMed: 7996857]
42. Ramirez-Solis R, Liu P, Bradley A. Chromosome engineering in mice. Nature 1995;378:720–724. [PubMed: 7501018]
43. Rogers T, Chandler D, Angelicheva D, Thomas PK, Youl B, et al. A novel locus for autosomal recessive peripheral neuropathy in the EGR2 region on 10q23. Am J Hum Genet 2000;67:664–671. [PubMed: 10915613]
44. Schneider A, Zhang Y, Guan Y, Davis LS, Breyer MD. Differential, inducible gene targeting in renal epithelia, vascular endothelium, and viscera of Mx1Cre mice. Am J Physiol Renal Physiol 2003;284:F411–417. [PubMed: 12529277]
45. Schon MP. Animal models of psoriasis - what can we learn from them? J Invest Dermatol 1999;112:405–410. [PubMed: 10201521]
46. Sharpless NE, DePinho RA. How stem cells age and why this makes us grow old. Nat Rev Mol Cell Biol 2007;8:703–713. [PubMed: 17717515]
47. Shu Z, Vijayakumar S, Chen CF, Chen PL, Lee WH. Purified human SUV3p exhibits multiple-substrate unwinding activity upon conformational change. Biochemistry 2004;43:4781–4790. [PubMed: 15096047]
48. Slijepcevic P. DNA damage response, telomere maintenance and ageing in light of the integrative model. Mech Ageing Dev 2007;129:11–16. [PubMed: 18063009]
49. Stepien PP, Margossian SP, Landsman D, Butow RA. The yeast nuclear gene suv3 affecting mitochondrial post-transcriptional processes encodes a putative ATP-dependent RNA helicase. Proc Natl Acad Sci U S A 1992;89:6813–6817. [PubMed: 1379722]
50. Sun LQ, Lee DW, Zhang Q, Xiao W, Raabe EH, et al. Growth retardation and premature aging phenotypes in mice with disruption of the SNF2-like gene, PASG. Genes Dev 2004;18:1035–1046. [PubMed: 15105378]
51. Szczesny RJ, Obriot H, Paczkowska A, Jedrzejczak R, Dmochowska A, et al. Down-regulation of human RNA/DNA helicase SUV3 induces apoptosis by a caspase- and AIF-dependent pathway. Biol Cell 2007;99:323–332. [PubMed: 17352692]
52. Taylor RW, Turnbull DM. Mitochondrial DNA mutations in human disease. Nat Rev Genet 2005;6:389–402. [PubMed: 15861210]
53. Terman A, Brunk UT. Aging as a catabolic malfunction. Int J Biochem Cell Biol 2004;36:2365–2375. [PubMed: 15325578]
54. Thomas PK, Kalaydjieva L, Youl B, Rogers T, Angelicheva D, et al. Hereditary motor and sensory neuropathy-russe: new autosomal recessive neuropathy in Balkan Gypsies. Ann Neurol 2001;50:452–457. [PubMed: 11601496]
55. Tyynismaa H, Mjosund KP, Wanrooij S, Lappalainen I, Ylikallio E, et al. Mutant mitochondrial helicase Twinkle causes multiple mtDNA deletions and a late-onset mitochondrial disease in mice. Proc Natl Acad Sci U S A 2005;102:17687–17692. [PubMed: 16301523]

56. Vasioukhin V, Degenstein L, Wise B, Fuchs E. The magical touch: genome targeting in epidermal stem cells induced by tamoxifen application to mouse skin. Proc Natl Acad Sci U S A 1999;96:8551–8556. [PubMed: 10411913]
57. Vennos EM, Collins M, James WD. Rothmund-Thomson syndrome: review of the world literature. J Am Acad Dermatol 1992;27:750–762. [PubMed: 1430398]
58. Vennos EM, James WD. Rothmund-Thomson syndrome. Dermatol Clin 1995;13:143–150. [PubMed: 7712640]
59. Wang X, Zinkel S, Polonsky K, Fuchs E. Transgenic studies with a keratin promoter-driven growth hormone transgene: prospects for gene therapy. Proc Natl Acad Sci U S A 1997;94:219–226. [PubMed: 8990189]
60. Wanrooij S, Luoma P, van Goethem G, van Broeckhoven C, Suomalainen A, et al. Twinkle and POLG defects enhance age-dependent accumulation of mutations in the control region of mtDNA. Nucleic Acids Res 2004;32:3053–3064. [PubMed: 15181170]
61. Warming S, Costantino N, Court DL, Jenkins NA, Copeland NG. Simple and highly efficient BAC recombineering using galK selection. Nucleic Acids Res 2005;33:e36. [PubMed: 15731329]
62. Xia YP, Zhao Y, Marcus J, Jimenez PA, Ruben SM, et al. Effects of keratinocyte growth factor-2 (KGF-2) on wound healing in an ischaemia-impaired rabbit ear model and on scar formation. J Pathol 1999;188:431–438. [PubMed: 10440755]
63. Zhu H, Conrad-Webb H, Liao XS, Perlman PS, Butow RA. Functional expression of a yeast mitochondrial intron-encoded protein requires RNA processing at a conserved dodecamer sequence at the 3′ end of the gene. Mol Cell Biol 1989;9:1507–1512. [PubMed: 2657398]

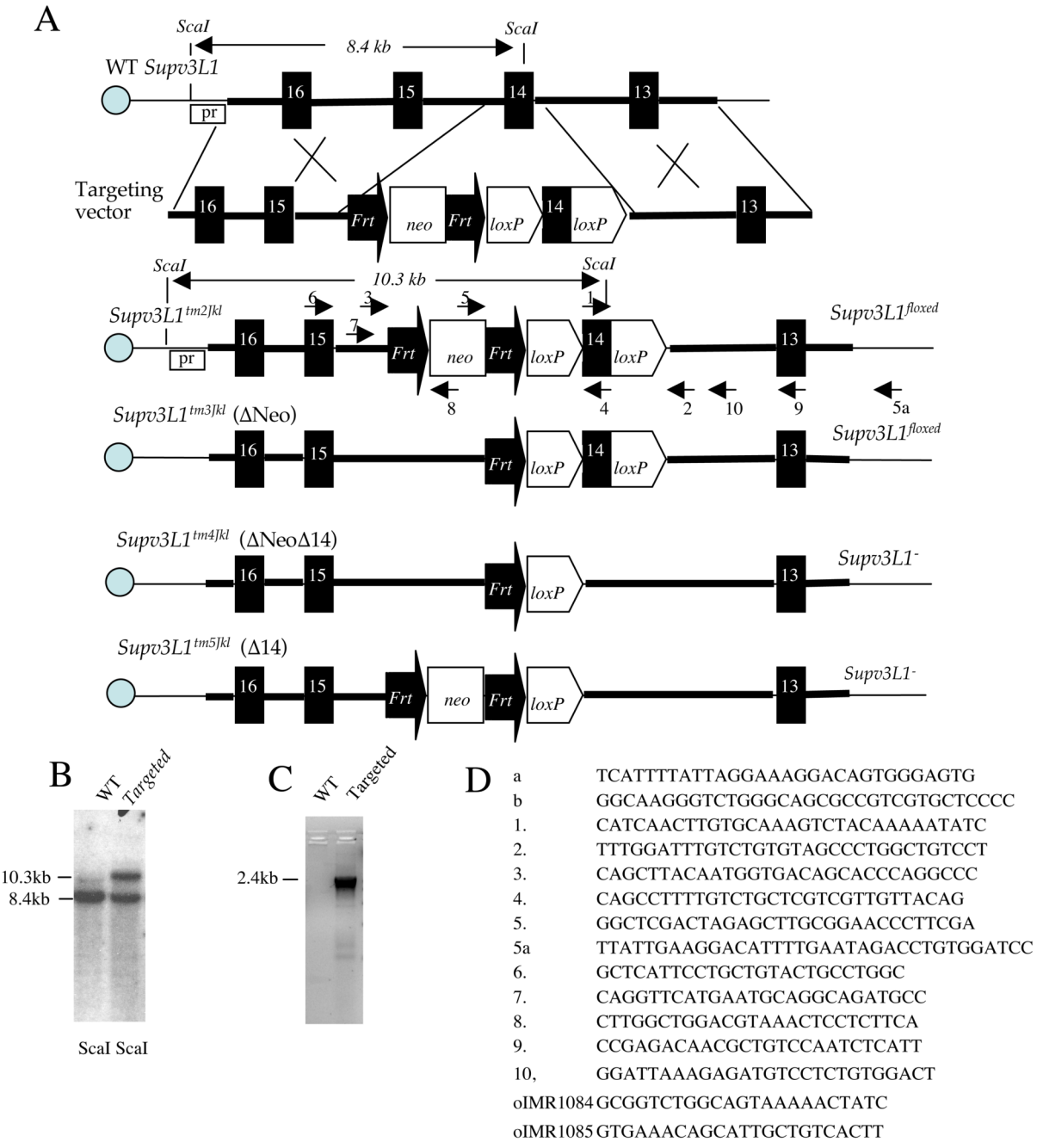

Figure 1.

Targeting the *Supv3L1* allele. (**A**) Genomic structure of the wild-type *Supv3L1* locus, targeting vector, and allelic modifications generated in this study. Regions of homology between the genome and vector are shown in bold. *ScaI*, *ScaI* restriction sites; Pr, probe used in Southern blotting; *Frt*, *frt sites; loxP*, *loxP* site; *Neo*, G418 resistance gene. Arrows indicate the positions of PCR primes. (**B**) Southern hybridization analysis of targeted ES cells showing a correct integration event at the 5′ arm. (**C)** PCR analysis of a targeted ES cell clones with primers 5 and 5a confirming a correct integration event at the 3′ arm. (**D**) Primers used for RCR analysis of the various *Supv3L1* alleles. Appropriate primer pair combinations allow the detection of all possible allele combinations. Primers oIMR1084 and oIMR1085 were used to detect the

Cre allele. (**E**) Sequence of exon 14. In some databases, mouse Supv3L1 is denoted as being composed of 16 exons, while in other databases, 15 exons. To avoid ambiguity, the sequence of exon used for floxing is provided.

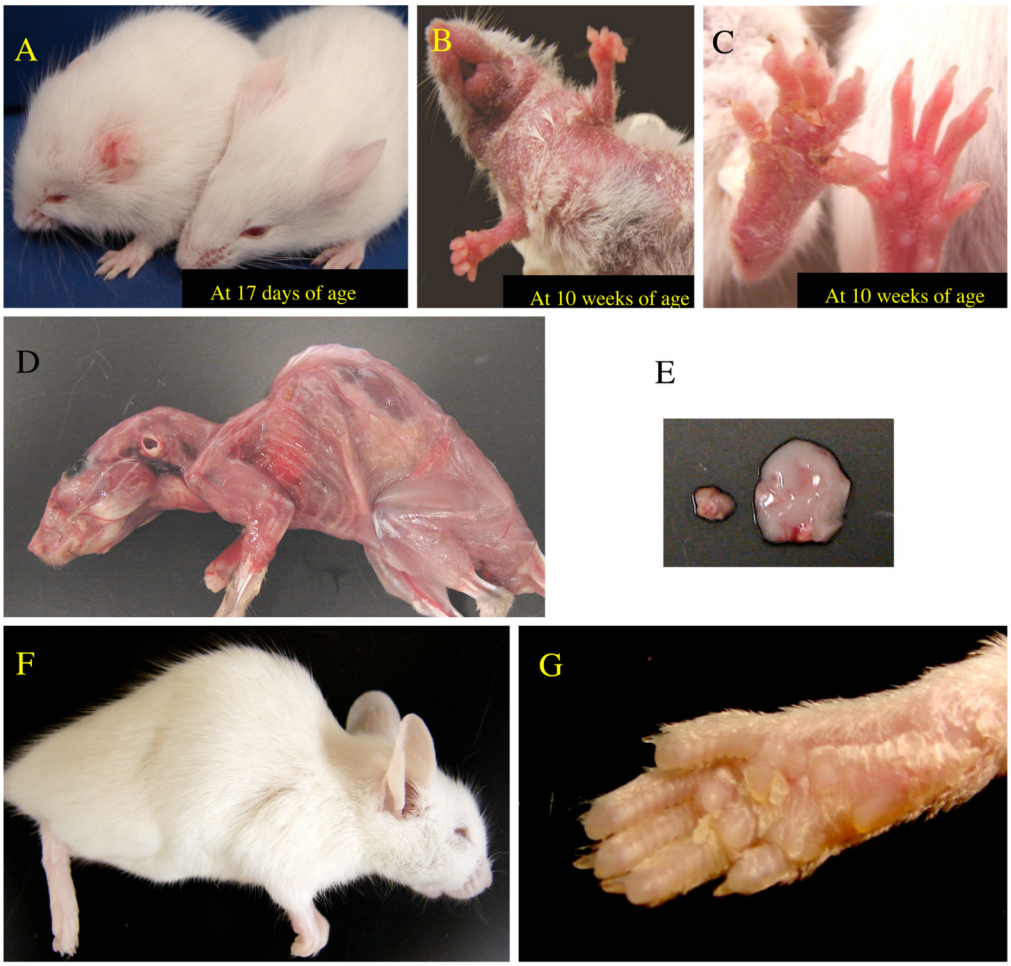

Figure 2.

Gross phenotypes of *Mx1*-Cre, *Supv3L1*$^{tm2Jkl/tm2Jkl}$, *Actb*-Cre *Supv3L1*$^{tm3Jkl/tm4Jkl}$ and *Actb*-Esr1/Cre *Supv3L1*$^{tm2Jkl/tm2Jkl}$ animals. (**A**) *Supv3L1*$^{tm2Jkl/tm2Jkl}$ animal at 17 days of age showing flattened and disfigured ears (left) next to a *Mx1*-Cre *Supv3L1*$^{tm2Jkl/+}$ littermate. (**B**) Abdominal alopecia of a *Mx1*-Cre *Supv3L1*$^{tm2Jkl/tm2Jkl}$ animal at 10 weeks of age. (**C**) Formation of scales on feet of a *Mx1*-Cre *Supv3L1*$^{tm2Jkl/tm2Jkl}$ animal at 10 weeks of age (left) relative to a normal mouse (right) of the same age. (**D**) Typical appearance of a *Actb*-Cre *Supv3L1*$^{tm3Jkl/tm4Jkl}$ animal without tamoxifen administration at the age of 10 weeks showing kyphosis, sarcopenia and no subcutaneous fat deposits. The same phenotype develops in *Actb*-Cre *Supv3L1*$^{tm2Jkl/tm2Jkl}$ mice (not shown). (**E**) Thymic atrophy in a *Actb*-Cre *Supv3L1*$^{tm3Jkl/tm4Jkl}$ animal (left) relative to a normal thymus (right) from a *Actb*-Cre *Supv3L1*$^{tm3Jkl/+}$ littermate of the same sex and age (female). (**F**) Kyphosis of a *Actb*-Esr1/Cre *Supv3L1*$^{tm2Jkl/tm2Jkl}$ animal after subcutaneous injection of tamoxifen. Note no apparent hair loss. (**G**) After subcutaneous injection of tamoxifen, about 35% of *Actb*-Esr1/Cre *Supv3L1*$^{tm2Jkl/tm2Jkl}$ mice develop scaling on their feet and tails but not on the body skin.

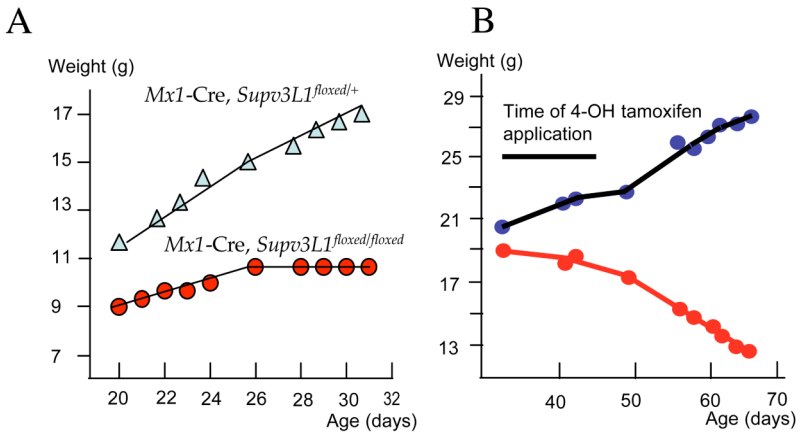

Figure 3.

Growth changes in *Mx1*-Cre *Supv3L1*$^{tm2Jkl/tm2Jkl}$ and *Actb*-Esr1/Cre *Supv3L1*$^{tm2Jkl/tm2Jkl}$ mice. (**A**) Weights of *Mx1*-Cre *Supv3L1*$^{tm2Jkl/tm2Jkl}$ and *Mx1*-Cre *Supv3L1*$^{tm2Jkl/+}$ mice recorded over a period of 11 days (average of three animals per genotype). (**B**) Weight loss of animals topically treated with 4-hydroxy tamoxifen: *Actb*-Esr1/Cre *Supv3L1*$^{tm2Jkl/tm2Jkl}$, red; *Actb*-Esr1/Cre, *Supv3L1*$^{tm2Jkl/+}$, blue. The data represent the average of three animals per genotype.

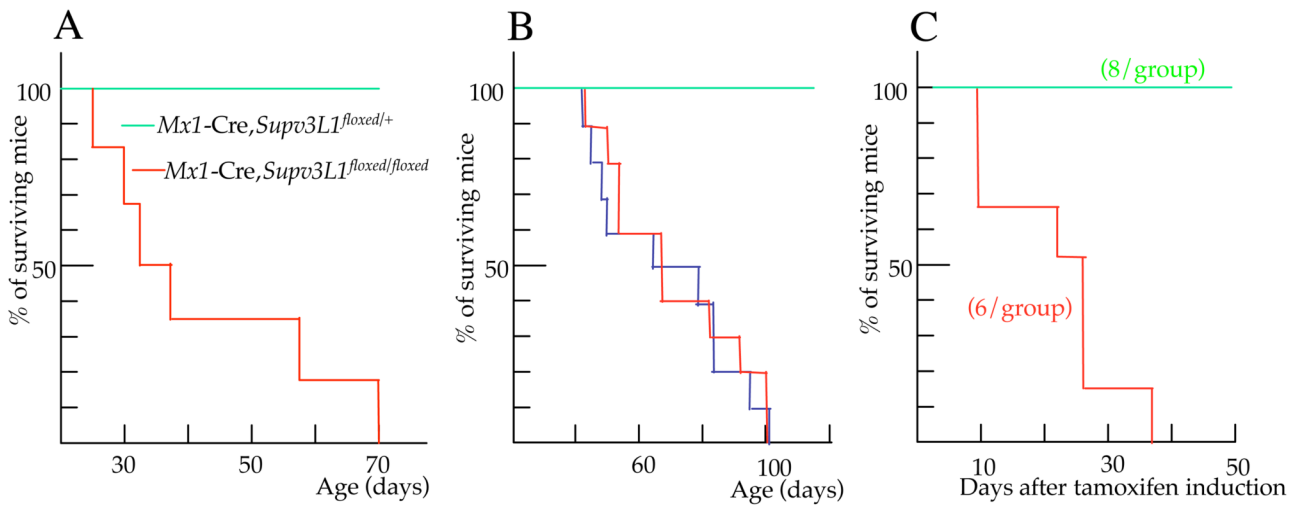

Figure 4.

Survival rates. (**A**) Survival curve of *Mx1*-Cre *Supv3L1*$^{tm2Jkl/+}$ and *Mx1*-Cre *Supv3L1*$^{tm2Jkl/tm2Jkl}$ mice (six animals per group). (**B**) Survival curve of *Actb-Esr1*/Cre, *Supv3L1*$^{tm3Jkl/+}$ and *Actb-Esr1*/Cre, *Supv3L1*$^{tm2Jkl/+}$ (controls) animals, green line; *Actb*-Cre *Supv3L1*$^{tm3Jkl/tm4Jkl}$, red line; *Actb*-Cre *Supv3L1*$^{tm2Jkl/tm2Jkl}$, blue line. Each group consisted of 9 animals. (**C**) Survival rates of *Actb*-Esr1/Cre *Supv3L1*$^{tm2Jkl/tm2Jkl}$ animals after tamoxifen administration (red line) relative to *Actb*-Esr1/Cre *Supv3L1*$^{tm2Jkl/+}$ (control) mice also injected with tamoxifen. Survival plots for *Actb*-Esr1/Cre *Supv3L1*$^{tm3Jkl/tm4Jkl}$ and *Actb*-Esr1/Cre *Supv3L1*$^{tm3Jkl/+}$ (control) animals were similar.

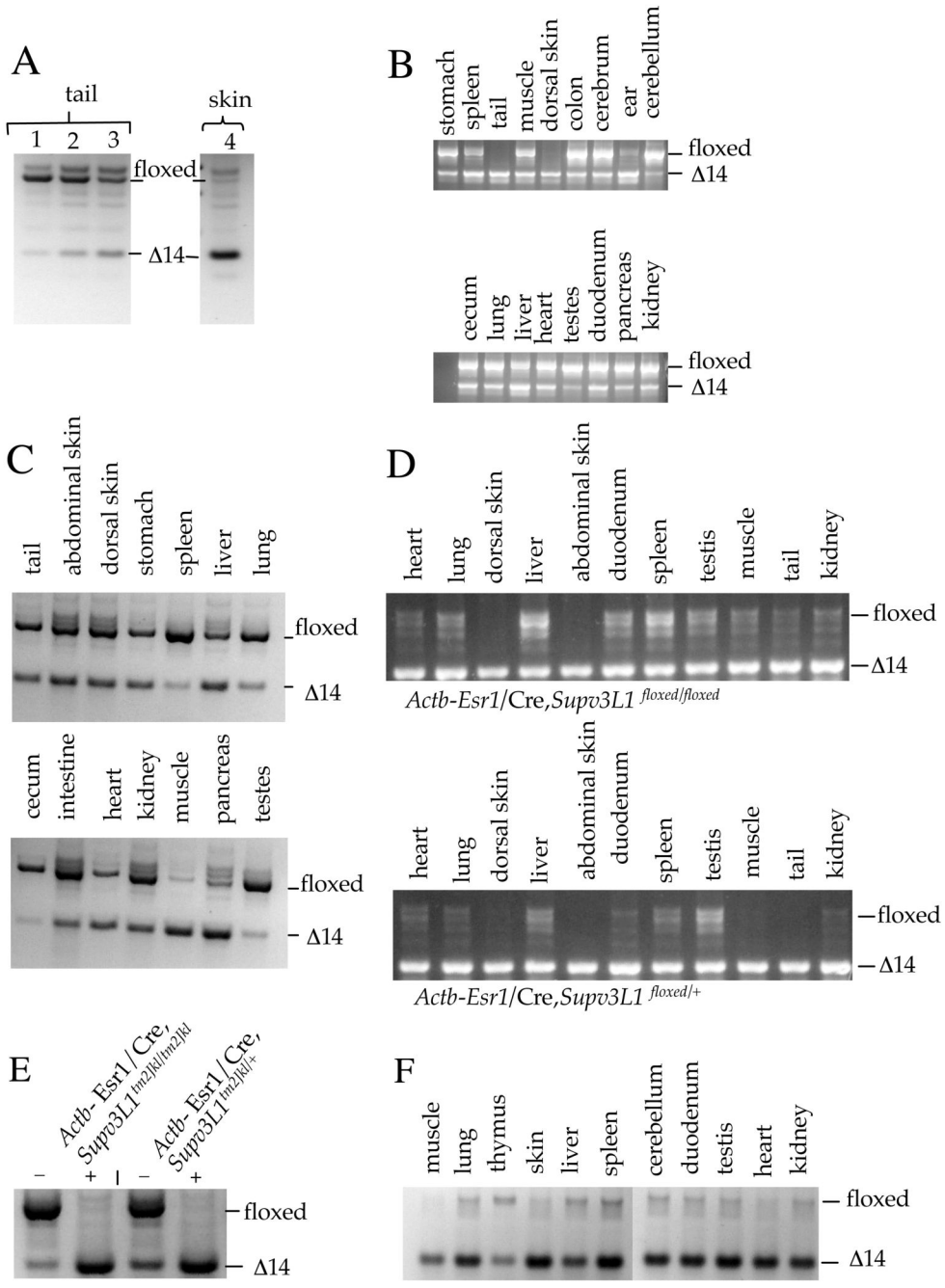

Figure 5.

The status of the floxed allele in mice of different genotypes. (**A**) Progressive conversion of the *floxed* allele into the Δ14 allele in a *Mx1*-Cre *Supv3L1*$^{tm2Jkl/tm2Jkl}$ mouse. Lanes 1–3, tail biopsies analyzed by PCR at ages of 14, 21 and 28 days, respectively. Lane 4, PCR performed on a skin sample collected at the time of death (37 days). (**B**) The status of the *floxed* allele in a *Mx1*-Cre *Supv3L1*$^{tm2Jkl/tm2Jkl}$ mouse at the time of death (10 weeks) showing different extents of deletion in different tissues. (**C**) The deletion status of the *floxed* allele in tissues of *Actb*-Cre *Supv3L1*$^{tm3Jkl/tm4Jkl}$ animals (without tamoxifen administration) at 10 weeks of age as determined by PCR. (**D**) The deletion status of the *floxed Supv3L1* alleles in different tissues of *Actb*-Esr1/Cre *Supv3L1*$^{tm2Jkl/tm2Jkl}$ and *Actb*-Esr1/Cre *Supv3L1*$^{tm2Jkl/+}$ animals after

subcutaneous tamoxifen administration. (**E**) The deletion status of the *Supv3L1* allele in the skin of animals before 4-hydroxy tamoxifen application (−) and after (+), as assessed by PCR. Note virtually compete deletion of exon 14 in both genotypes. (**F**) The deletion status of the *floxed Supv3L1* alleles in different tissues of *Actb*-Esr1/Cre *Supv3L1*$^{tm2Jkl/tm2Jkl}$ animals after topical 4-hydroxy tamoxifen administration. Topical applications of 4-hydroxy tamoxifen using *Actb*-Esr1/Cre *Supv3L1*$^{tm3Jkl/tm4Jkl}$ and *Actb*-Esr1/Cre, *Supv3L1*$^{tm3Jkl/+}$ animals led to the same response.

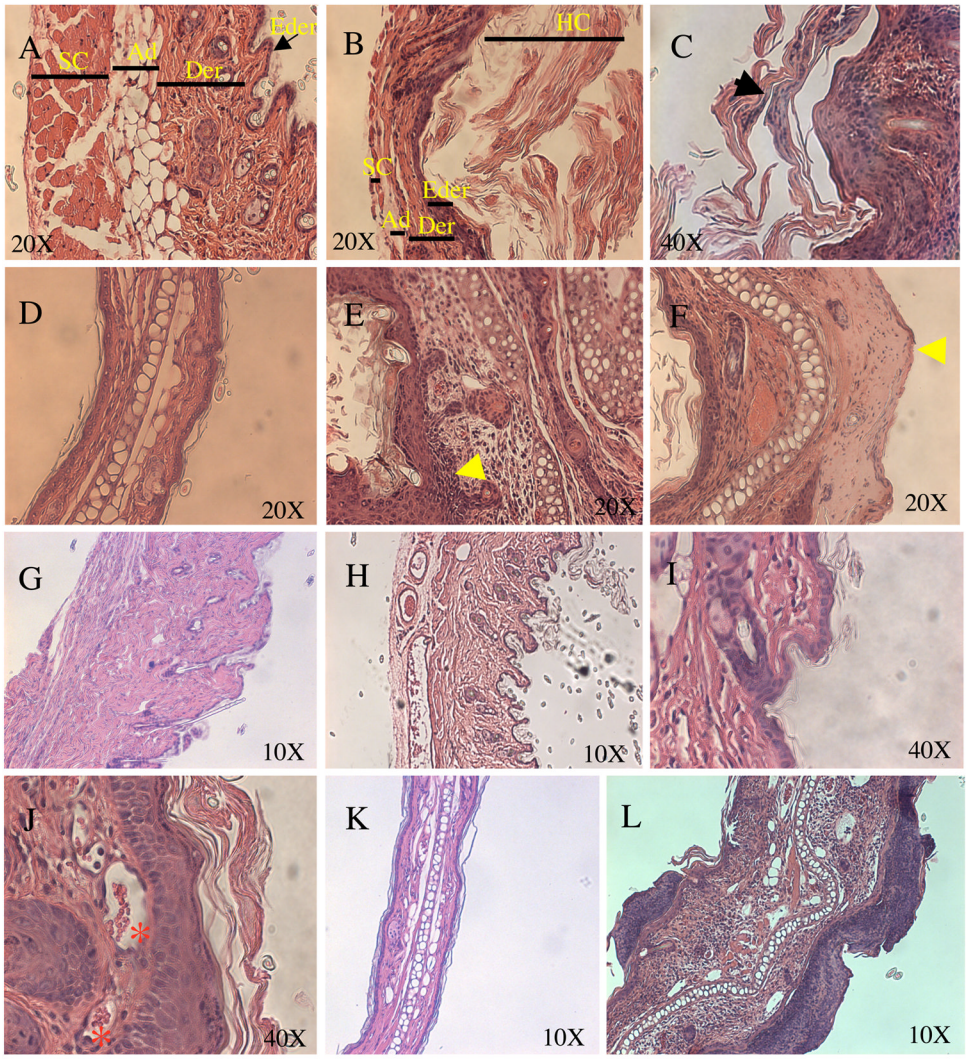

Figure 6.

H&E stained cross-sections of the skin and ears. (**A**) Normal skin at 10 weeks of age from *Mx1*-Cre *Supv3L1*$^{tm2Jkl/+}$ mouse. Ad, adipose layer; Der, dermis; Eder, epidermis; SC, subcutaneous muscle fibers. (**B**) Skin from an age-matched *Mx1*-Cre *Supv3L1*$^{tm2Jkl/tm2Jkl}$ animal. HC, hyperkeratosis. Note the thickened epidermis, severe hyperkeratosis, dystrophic dermis, lack of sebaceous glands, and almost total absence of adipose and muscle layers. (**C**) Higher power magnification of the skin from *Mx1*-Cre *Supv3L1*$^{tm2Jkl/tm2Jkl}$ animal showing parakeratosis (arrow) and scaling. (**D**) Cross-section through a normal ear of an *Mx1*-Cre *Supv3L1*$^{tm2Jkl/+}$ animal at 10 weeks of age. (**E**) Cross-section through an ear of an age-matched *Mx1*-Cre *Supv3L1*$^{tm2Jkl/tm2Jkl}$ animal showing disfigured morphology, thickened epidermis, hyperkeratosis, and neutrophilic microabscesses (arrowhead). (**F**) Another *Mx1*-Cre *Supv3L1*$^{tm2Jkl/tm2Jkl}$ cross-section showing a hyperkeratotic area with absent epidermal cells (arrowhead). (**G**) H&E stained skin section of a *Actb*-Cre *Supv3L1*$^{tm2Jkl/tm2Jkl}$ animal at the age of 12 weeks. (**H**) Dorsal skin from a *Actb*-Cre *Supv3L1*$^{tm2Jkl/tm2Jkl}$ animal injected subcutaneously with tamoxifen at the age of 25 days. Note the absence of adipose tissue, paucity of subcutaneous muscle, dilated blood vessels and mild hyperkeratosis. (**I**) Skin from the control animal (*Actb*-Esr1/Cre *Supv3L1*$^{tm2Jkl/+}$) topically treated with 4-hydroxy tamoxifen. (**J**) A skin sample from a *Actb*-Esr1/Cre *Supv3L1*$^{tm2Jkl/tm2Jkl}$ animal after topical 4-hydroxy

tamoxifen treatment. Note hyperkeratotic and parakeratotic changes along with a significantly thickened epidermal layer of cells. Dilated blood vessels in the dermal layer are marked with asterisks. (**K**) Ear crossection of a control KRT14-Cre/Esr1 *Supv3L1*$^{tm3Jkl/+}$ mouse after subcutaneous administration of tamoxifen. Biopsy was taken 4 weeks after subcutaneous administration was completed. (**L**) Ear crossection of a KRT14-Cre/Esr1 *Supv3L1*$^{tm3Jkl/tm4Jkl}$ littermate of the same sex and age after subcutaneous administration of tamoxifen. Note atrophy of hair follicles, sweat glands, thickening of epidermis, hyperkeratosis, dilation of blood vessels, and infiltrative changes.

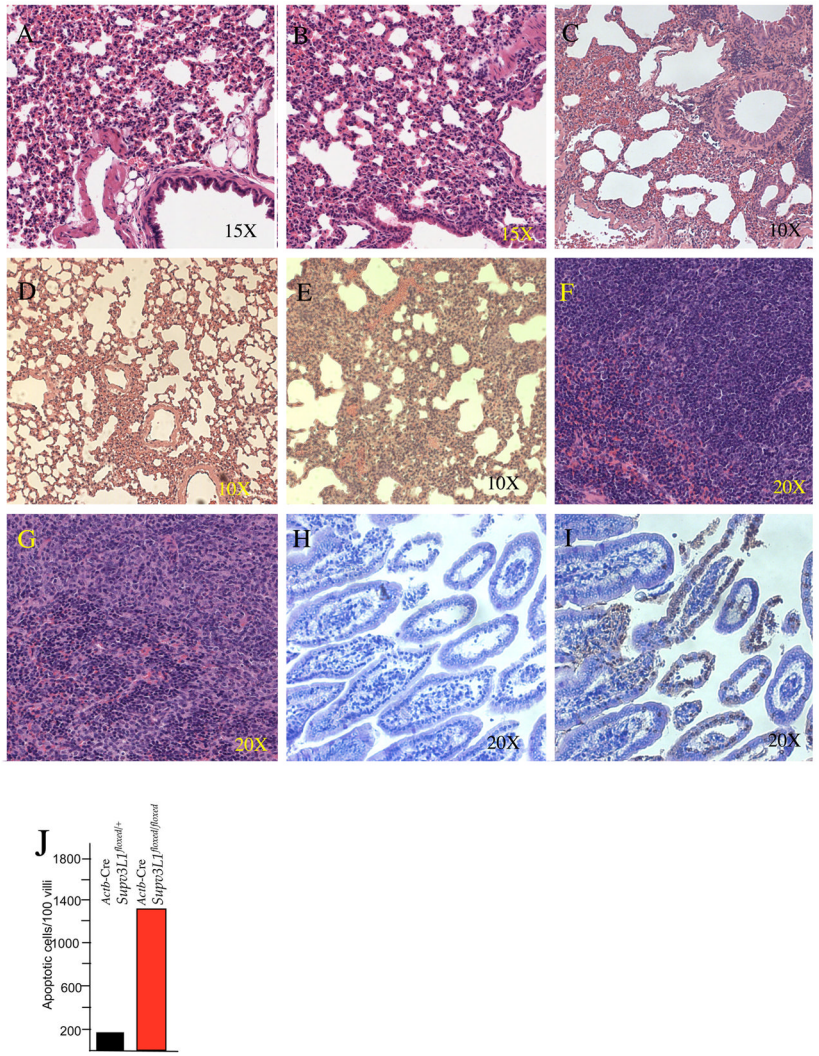

Figure 7.

Histology of the lung, spleen, and duodenum. (**A**) *Mx1*-Cre *Supv3L1*$^{tm2Jkl/+}$ and (**B**) *Mx1*-Cre *Supv3L1*$^{tm2Jkl/tm2Jkl}$ lung at 7 weeks. Note an increased number of inflammatory cells and edema. (**C**) H&E stained section of the lung from *Actb*-Cre *Supv3L1*$^{tm2Jkl/tm2Jkl}$ animal at the age of 12 weeks. Note an increased number of inflammatory cells, congestion and edema. (**D**) Lung from a control *Actb*-Cre *Supv3L1*$^{tm2Jkl/+}$ animal injected subcutaneously with tamoxifen at the age of 25 days. (**E**) Lung from a *Actb*-Cre *Supv3L1*$^{tm2Jkl/tm2Jkl}$ animal injected subcutaneously with tamoxifen at the age of 25 days. Note the presence of increased inflammatory cells, congestion, and edema. (**F**) H&E-stained section of the spleen from a control *Mx1*-Cre *Supv3L1*$^{tm2Jkl/+}$ mouse. (**G**) *Mx1*-Cre *Supv3L1*$^{tm2Jkl/tm2Jkl}$ spleen at 7 weeks. Note splenic atrophy. (**H**) TUNEL assay performed on a crossection of the duodenum from a *Actb*-Cre *Supv3L1*$^{tm2Jkl/tm2Jkl}$ control littermate injected subcutaneously with tamoxifen at the age of 25 days. Note the low number of TUNEL-positive cells. (**I**) The same assay performed on the duodenum from a *Actb*-Cre *Supv3L1*$^{tm2Jkl/tm2Jkl}$ animal also injected with tamoxifen. Note numerous TUNEL-positive cells. (**J**) Quantification of apoptotic cells in panels (H) and (I).

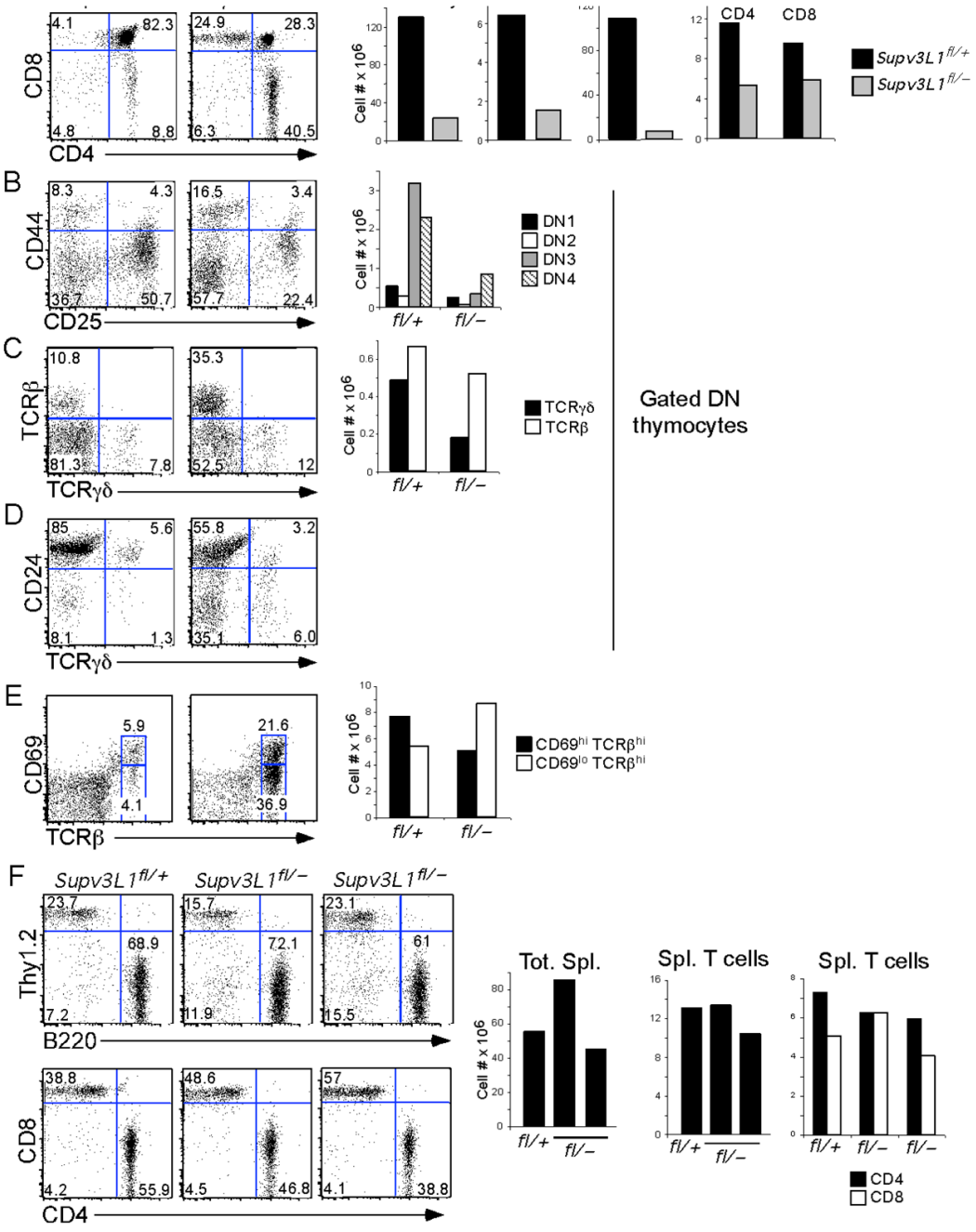

Figure 8.

Flow cytometric analysis of thymic T cell progenitors and mature spleen T cells. Thymocytes (**A–E**) and splenocytes (**F**) were analyzed by flow cytometry using monoclonal antibodies reactive with the following differentiation antigens (**A–F**): CD4, CD8, CD69, TCRβ, CD25, CD44, TCRγδ, CD24, Thy1.2, and B220. Gate frequencies are listed in the quadrants of the histograms. Absolute numbers of populations were calculated from gate frequencies and are represented graphically on the right side of the figure. Tot. Thy.: Total thymocyte, DP: double positive, DN: double negative, SP: single positive, and Tot. Spl.: Total splenocyte. *Supv3L1*$^{fl/+}$ and *fl*/+ refer to a control, tamoxifen injected *Actb*-Esr1/Cre *Supv3L1*$^{tm2Jkl/+}$ mice

displaying no phenotype. *Supv3L1*$^{fl/-}$ and *fl*/$^{-}$ refer to *Actb*-Esr1/Cre *Supv3L1*$^{tm3Jkl/tm4Jkl}$ and *Actb*-Esr1/Cre *Supv3L1*$^{tm2Jkl/tm2Jkl}$ mice that display phenotypes after tamoxifen induction.